

# Dual-band CPW rectenna for low input power energy harvesting applications

 ISSN 1751-858X  
 Received on 11th January 2020  
 Revised 9th May 2020  
 Accepted on 1st June 2020  
 doi: 10.1049/iet-cds.2020.0013  
 www.ietdl.org

Mohamed Aboualalaa<sup>1</sup> ✉, Islam Mansour<sup>2</sup>, Adel B. Abdelrahman<sup>3,4</sup>, Ahmed Allam<sup>3</sup>, Mohamed Ab-zahhad<sup>3,5</sup>, Hala Elsadek<sup>1</sup>, Ramesh K. Pokharel<sup>6</sup>

<sup>1</sup>Microstrip Circuits Department, Electronics Research Institute, Cairo, Egypt

<sup>2</sup>Electrical Engineering Department, Shoubra Faculty of Engineering, Benha University, Cairo 11629, Egypt

<sup>3</sup>Communications and Computer Engineering, Egypt-Japan University of Science and Technology (E-JUST), New Borg El Arab City, Alexandria, Egypt

<sup>4</sup>Electrical Engineering Department, Faculty of Engineering, South Valley University, Qena, Egypt

<sup>5</sup>Electrical Engineering Department, Faculty of Engineering, Assiut University, Assiut, Egypt

<sup>6</sup>Faculty of Information Science and Electrical Engineering, Kyushu University, Fukuoka, Japan

✉ E-mail: mohamed.ali@ejust.edu.eg

**Abstract:** A dual-frequency band low input power rectenna is proposed in this study. The rectenna is comprised of a co-planar waveguide (CPW) rectifier integrated with a rectangular split ring antenna loaded by a spiral strip line. A single diode series connection topology is used to miniaturise the losses at low input power. A spiral coil in addition to two short circuit stubs are used as a matching network for maximum power transfer between the antenna and the rectifying circuit. The proposed rectenna operates at low input power with relatively high measured RF-DC conversion efficiency up to 74% at input power of  $-6.5$  dBm at the first resonant frequency  $f_1 = 700$  MHz and 70% at  $-4.5$  dBm at the second operating frequency  $f_2 = 1.4$  GHz with a resistive load of  $1.9$  k $\Omega$ . The measured rectenna sensitivity (the rectenna ability to receive low power with acceptable conversion efficiency) reaches up to  $-20$  dBm with a conversion efficiency of 47 and 36% at  $f_1$  and  $f_2$ , respectively, and a DC output voltage of  $0.18$  V. The measured efficiency is over 50% from  $-18$  to  $-3.5$  dBm and from  $-15$  to  $-1.5$  dBm at  $f_1$  and  $f_2$ , respectively.

## 1 Introduction

In the last few years, there has been a growing interest in wireless power transmission (WPT). WPT can be categorised into three different categories: near-field inductive or resonant coupling, far-field directive powering and far-field ambient wireless energy harvesting. Near-field WPT offers a solution to short-range powering, it becomes widely commercialised for several wireless applications [1–4]. Nevertheless, near-field WPT suffers from a severe issue with regard to the transmitting distance; it covers only a very short range distance (few centimetres), therefore this limits its applications. On the other hand, far-field dedicated source powering or free ambient powering can overcome this problem because of the long-distance charging capability. Several studies are introduced in wireless energy harvesting [5–7]. Although the focusing is on wireless energy harvesting, there are many obstacles in the way of free source energy harvesting. One of the main issues is low input power levels of the ambient energy. Consequently, there are many research papers introduced for rectennas at low input power levels.

In [6], a compact co-planar waveguide (CPW)-fed rectenna using single-stage Cockcroft Walton rectifier and L-shaped impedance matching network is presented. The RF-DC conversion efficiency is 68% with a received input signal power of 5 dBm at 2.45 GHz. This rectenna has conversion efficiencies around 48 and 19% at  $-10$  and  $-20$  dBm, respectively. A compact dual-band rectenna is proposed in [8]. The rectenna has a conversion efficiency of 37 and 30% at 915 MHz and at 2.45 GHz, respectively, at input power of  $-9$  dBm with resistive load of  $2.2$  k $\Omega$ . A dual-band rectenna using Yagi antenna for low input power applications is introduced in [9]. The rectenna offers an acceptable values for the rectenna efficiencies, it reaches up to 34% at 1.84 GHz and 30% at 2.14 GHz for input power level of  $-20$  dBm. A combination between the solar energy and RF energy harvesting is discussed in [10]. This solar rectenna achieves RF-DC conversion efficiency of 15% with input power of  $-20$  dBm at

850 MHz and 2.45 GHz. In [11], a 130 nm CMOS rectifier is proposed for ultra-low input power. It consists of ten stages to give the maximum efficiency of 42.8% at  $-16$  dBm input power and output DC voltage of 2.32 V at a resistive load of  $0.5$  M $\Omega$ . A multiport rectenna system is introduced in [12]. The rectenna harvests from GSM-900 and GSM-1800 frequency bands. It has a peak conversion efficiency of 38.1 and 34% at 0.9 and 1.8 GHz, respectively, when the input power was  $-20$  dBm. A triple-band energy harvesting system is discussed in [13]. This rectenna works at GSM-1800, UMTS-2100 and WiFi systems with maximum RF-to-DC conversion efficiency of 25.3, 27.9 and 19.3% at GSM-1800, UMTS-2100 and WiFi, respectively, with an input power of  $-20$  dBm.

Also, there are many low input power rectennas used for energy harvesting applications [14–17]. However, in this paper, a low input power CPW dual-band rectenna is introduced with high RF-DC conversion efficiency which reach up to 74 and 70% at  $-6.5$  and  $-4.5$  dBm, respectively, with high sensitivity which reach  $-20$  dBm with high conversion efficiency of 47 and 36%. Firstly, the CPW antenna is designed, fabricated and measured separately to check the antenna performance. Then, the rectifier and the matching scheme between the antenna and the rectifying circuit are also designed and tested independently. Finally, the integration between the antenna and rectifier is done on the same PCB substrate. Rectenna is usually used as a power unit integrated with an electronic device. Therefore, CPW structure is chosen to facilitate the interconnection between the rectenna and the other planar electronics circuits. The antenna has been simulated using ANSYS high frequency structure simulator, while the rectifier as well as the matching circuit have been simulated by co-simulation in Keysight advanced design system. Then, the antenna has been integrated with the rectifying circuit to form the rectenna. The simulation and measurement results of the rectenna show good agreement. The designated rectenna is proposed to harvest wireless

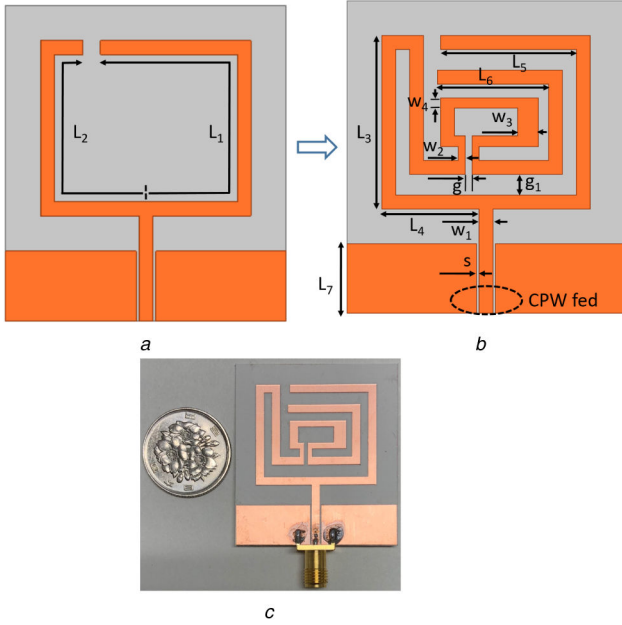


**Fig. 1** Antenna structure  
(a) CPW RSR design, (b) Antenna geometry, (c) Photograph of the fabricated antenna prototype

$L_1 = 53.5$  mm,  $L_2 = 36$  mm,  $L_3 = 25$  mm,  $L_4 = 14$  mm,  $L_5 = 19.5$  mm,  $L_6 = 16$  mm,  $L_7 = 10$  mm,  $W_1 = 2$  mm,  $W_2 = 1$  mm,  $W_3 = 3$  mm,  $W_4 = 1.5$  mm,  $g_1 = 3$  mm,  $g_2 = 1$  mm,  $S = 0.4$  mm,  $L_1 = 7.5$  mm,  $L_2 = 12$  mm,  $L_3 = 1.4$  mm,  $W_1 = 4.6$  mm,  $W_2 = 6$  mm,  $g_1 = 0.36$  mm,  $g_2 = 1.7$  mm,  $S = 7.6$  mm

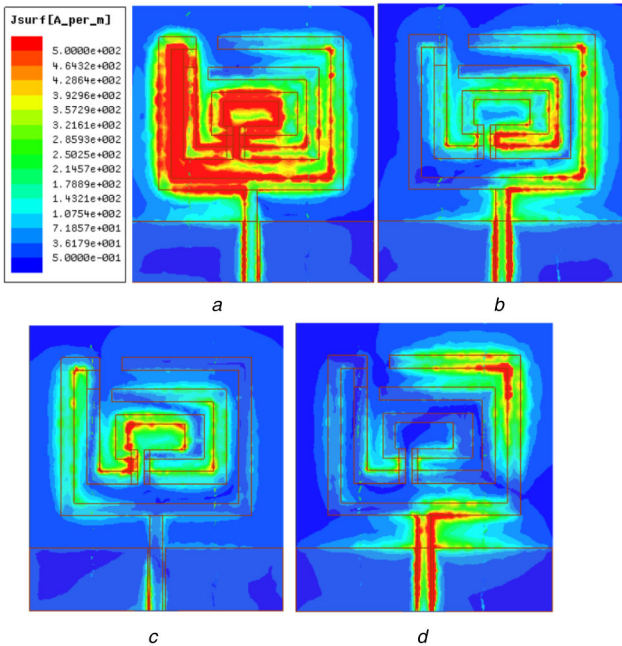


**Fig. 2** Surface current distribution at  
(a)  $f_1$ , (b)  $f_2$ , (c)  $f_3$ , (d)  $f_4$

energy from cellular mobile LTE (700 MHz band) and IMT (International Mobile Telecommunications, 1400 MHz band).

## 2 Receiving antenna

### 2.1 Antenna structure

Fig. 1a shows a rectangular split ring (RSR) with a length of ( $L_1 + L_2$ ) 89.5 mm which is excited by a CPW feed. The RSR is connected with spiral strip line (SSL) as illustrated in Fig. 1b to form the CPW quad-band antenna. CPW feed is adjusted to give around  $50\Omega$  input impedance for matching with feeding launcher impedance and assuring maximum power transfer between the

connector and the antenna. The proposed antenna is designed on Rogers Duroid RO3003 with substrate thickness ( $h$ ) of 0.76 mm, a relative permittivity ( $\epsilon_r$ ) of 3, a dielectric loss tangent ( $\tan\delta$ ) of 0.0013 and a copper thickness ( $t$ ) of 0.017 mm. The antenna geometrical parameters are shown in Fig. 1. The fabricated prototype of the proposed antenna is also shown in Fig. 1c.

### 2.2 Antenna reflection coefficient

The antenna has four operational frequency bands due to the combination between RSR and SSL with CPW feeding. Fig. 2 illustrates the surface current distribution at the four resonant frequencies  $f_1 = 0.7$  GHz,  $f_2 = 1.4$  GHz,  $f_3 = 2.78$  GHz and  $f_4 = 3.18$  GHz. As shown in Fig. 2, the resonant frequency  $f_1$  radiates from the total length of the RSR and SSL which is the longest current path to give the lower frequency band, while the resonant frequency  $f_2$  is propagating because of the strong coupling between RSR and SSL. On the other hand, the length of the SSL and the right (longer) branch of RSR are responsible for  $f_3$  and  $f_4$ , respectively, as depicted in Figs. 2c and d. Fig. 3 displays the comparison between the simulated and measured results of the antenna reflection coefficient  $|S_{11}|$ . The antenna impedance fractional bandwidths are 2.8, 3, 9.5 and 11% at  $f_1$ ,  $f_2$ ,  $f_3$  and  $f_4$ , respectively.

### 2.3 Antenna radiation characteristics

The  $E$ -plane and  $H$ -plane simulated and measured radiation patterns for co-polarisation and cross-polarisation at the frequencies of  $f_1$  and  $f_2$  are demonstrated in Fig. 4 which are the two bands used with the dual-band rectifier to get the dual-band rectenna. The antenna has realised gain values of 3.5, 3.8, 4.2, 4.6 dBi, and the radiation efficiency, at the same frequencies, are 89, 88, 91, 94%. The system shown in Fig. 5 is used in the radiation pattern measurements of the proposed antenna. It is clear from the radiation pattern results that one plane is omnidirectional, while the other plane is isotropic. Hence, this CPW monopole antenna can be used with ambient energy harvesting applications.

## 3 Rectifier design

### 3.1 Single band CPW rectifier

The rectifier has a single diode (Schottky barrier diode) series connection topology, which is the best topology for low received power applications [18, 19] as shown in Fig. 6a. A co-planar GSG (ground signal ground) structure is used for this design. After the rectifying stage, a shunt capacitor ( $C_p = 100$  pF, Murata C1H101FA16D) is used for DC output voltage smoothing and bypassing the higher order harmonics. Hence,  $C_p$  should be large enough to make a smoothing. We usually use it around 100pF. When  $C_p$  is over 100 pF, the increase in the value of  $C_p$  has a slight effect on the output results. The diode (Skyworks SMS 7630-061) and the capacitor models are included in the simulation study. The input impedance of the rectifying circuit shown in Fig. 6a is  $Z_{rec} = 8.9 - j43.1\Omega$  at resonance frequency of 1 GHz and output resistance of  $R_L = 500\Omega$ . To achieve a matching between  $Z_{rec}$  and  $50\Omega$  port input impedance, the first step is that a series inductance should be inserted with  $Z_{rec}$  to move the value of  $Z_{rec}$  upward in the direction of increasing inductive reactance on a Z-circle on the Smith chart. The equivalent impedance of the rectifier becomes  $Z_{rec}$ . Then,  $Z_{rec}$  needs to go through a Y-circle on the Smith chart to interact with the centre point of the Smith chart, which is the  $50\Omega$  matching point, in order to achieve that a short circuit stub is connected in parallel with  $Z_{rec}$  to obtain the whole equivalent circuit for the rectifier in addition to the matching circuit is equal to  $50\Omega$ . The matching circuit depicted in Fig. 6b is used for the matching. It comprises of series lumped inductor in addition to a parallel short circuit stub. Smith chart also illustrates the above-mentioned matching steps. In order to minimise the losses at the required low input power range, a spiral inductor, with a number of

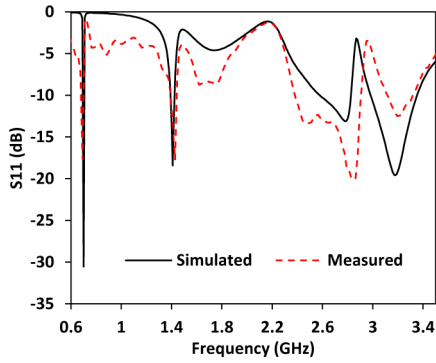


Fig. 3 Measured and simulated reflection coefficient

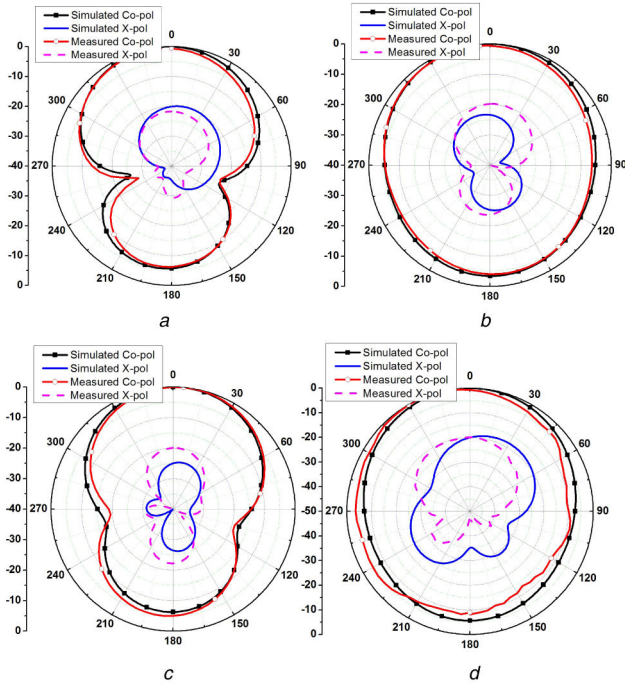


Fig. 4 Measured and simulated results of 2D radiation patterns for (a) E-plane at  $f_1$ , (b) H-plane at  $f_1$ , (c) E-plane at  $f_2$ , (d) H-plane at  $f_2$

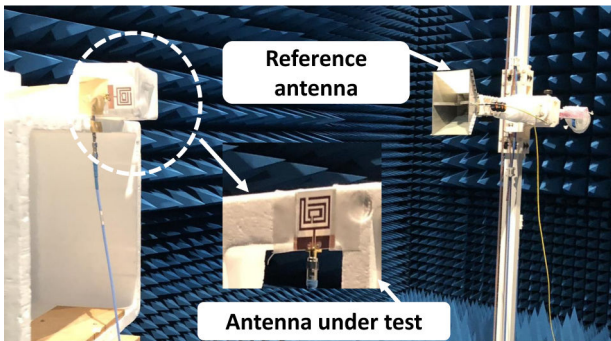


Fig. 5 Radiation pattern measurement system

turns 2.5, is used to achieve the matching instead of using a lumped inductor as shown in Fig. 7. Fig. 8a shows the RF-DC conversion efficiency as well as DC output voltage for this rectifier. As can be seen from the figure, the maximum value of the conversion efficiency is 69% at  $-4$  dBm. Hence, this rectifier can be used for low input power applications. The rectifier achieved good matching with a slight shift in the operating frequency as presented in Fig. 8b

### 3.2 Dual-band CPW rectifier

Using the same topology for the previously-mentioned single-band rectifier and adding another parallel short circuit stub to achieve

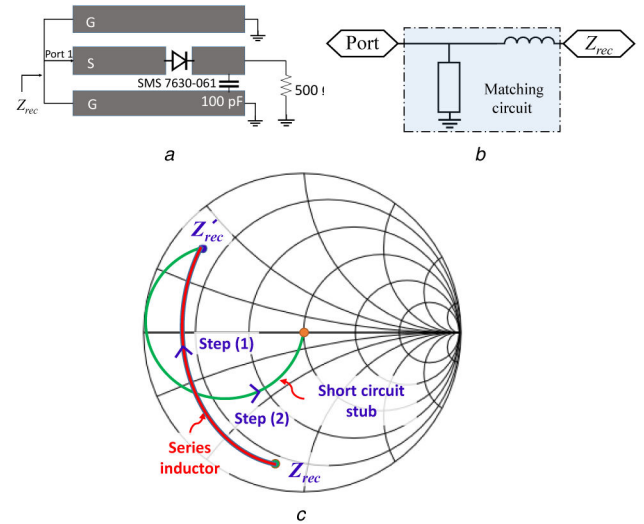


Fig. 6 Rectifier characterisation and matching (a) Diode series topology, (b) Matching circuit, (c) Matching steps illustrated on Smith chart

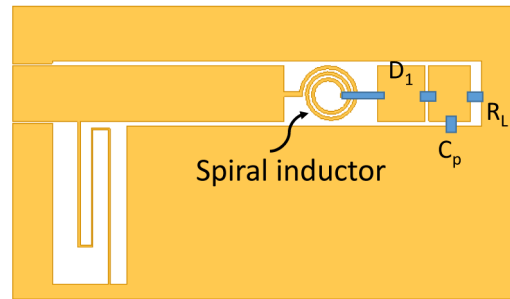


Fig. 7 Single-band rectifier geometry

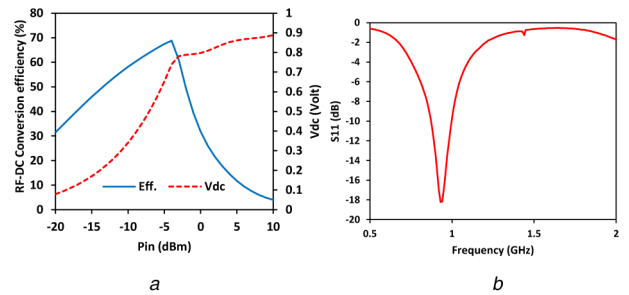
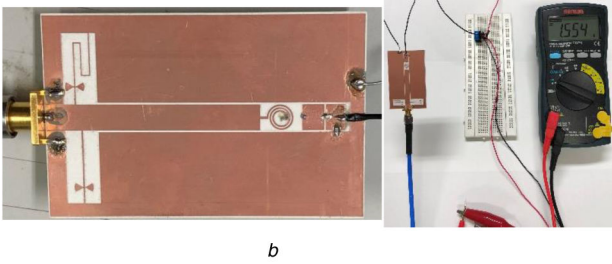
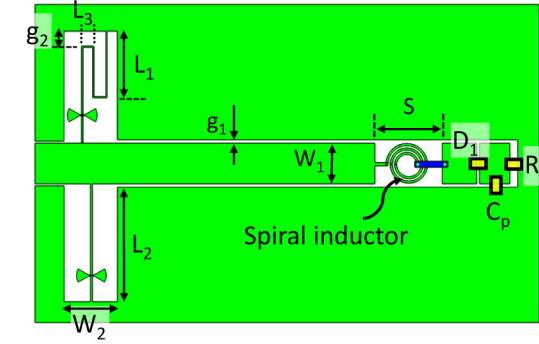


Fig. 8 Single rectification simulated results (a) RF-DC conversion efficiency and DC output voltage, (b) Reflection coefficient

dual-band rectification as illustrated in the geometry shown in Fig. 9a. Each separate short-circuit stub connected with the spiral inductor operates as a matching circuit for single frequency band, so the two stubs connecting with the spiral inductor control the matching for dual band (at  $f_1 = 0.7$  GHz and  $f_2 = 1.4$  GHz). Radial stubs are connected with the two short circuit stubs to give a high degree of freedom in adjusting the rectifier matching. The rectifier was designed and fabricated using the same material of the antenna substrate (RT/Duroid 3003). The fabricated prototype in addition to the measurement setup of the rectifier circuit is depicted in Fig. 9b. The measured and simulated reflection coefficient results at the two bands are illustrated in Fig. 10a. The rectifier presents good measured results of the RF-DC conversion efficiency and the DC output voltage at both frequencies. The measured conversion efficiencies are 72 and 67.5% at  $f_1$  and  $f_2$ , respectively. The measured RF-DC conversion efficiency can be obtained by

$$\eta_{\text{RF-DC}} = \frac{V_L^2}{R_L P_{\text{in}}} \times 100 \quad (1)$$



**Fig. 9 Dual-band rectifier**  
 (a) Rectifier geometry, (b) Photograph of the fabricated prototype of the rectifier as well as rectifier measurement setup

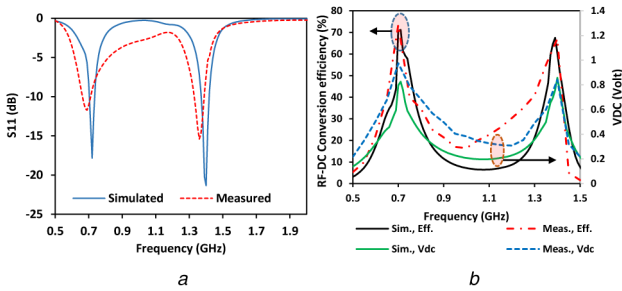


**Fig. 10 Dual rectification measured and simulated results**  
 (a) Reflection coefficient, (b) RF-DC conversion efficiency and DC output voltage

where  $V_L$  is the DC output voltage on the resistor  $R_L$  and  $P_{in}$  is the input power level generated by a signal generator.

Simulated and measured results of the conversion efficiency and the output voltage for the rectifier versus varied input power signal level are shown in Fig. 11a and are found generally in good agreement. The value of DC voltage components at the resonant frequency and the first and second harmonics are very low (below  $-20$  dB for the first three modes) as revealed in Fig. 11b, which indicates that  $C_p$  in this rectifier topology is chosen with optimal value and there is no need for DC output filter.

A parametric analysis of the conversion efficiency as well as the DC output voltage is carried out at different values of the load resistor ( $R_L$ ) and with varied received signal power from  $-20$  to  $10$  dBm at the two frequencies  $f_1$  and  $f_2$  as shown in Figs. 12 and 13 to observe the rectifier performance with variable operating parameters. It is clearly noticed that the rectifier can work efficiently at different values of  $R_L$ . However, the efficiency and the DC voltage increase with increasing  $R_L$  till  $2$  k $\Omega$ . After that, the output voltage value increases slightly whereas the efficiency tends to be fixed. After the optimisation, the optimal value of the  $R_L$  to give high conversion efficiency with good matching was found  $1.9$  k $\Omega$ .

#### 4 Rectenna measurements

In order to obtain higher values of the RF-DC conversion efficiency, the matching circuit has been optimised and stepped impedance transmission line is used and the number of turns of the spiral coil is changed to be 2.75 turns to improve the matching

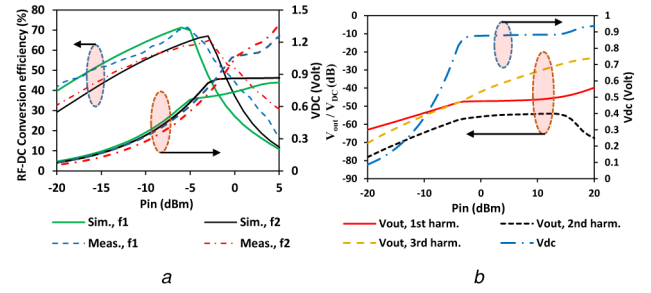


**Fig. 11 Measured and simulated results for dual-band rectification**  
 (a) RF-DC conversion efficiency and DC output voltage versus received input power, (b) Output voltage at different frequency modes compared with DC output voltage

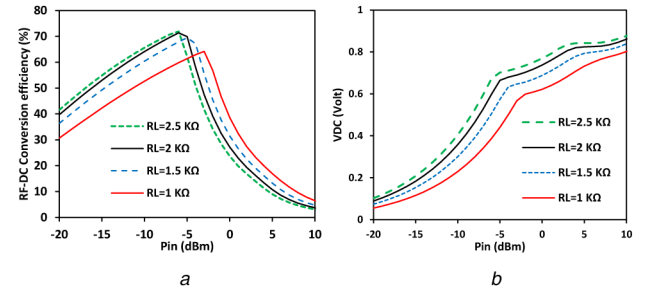


**Fig. 12 Study of changing  $R_L$  at  $f_1$**   
 (a) RF-DC conversion efficiency, (b) DC output voltage

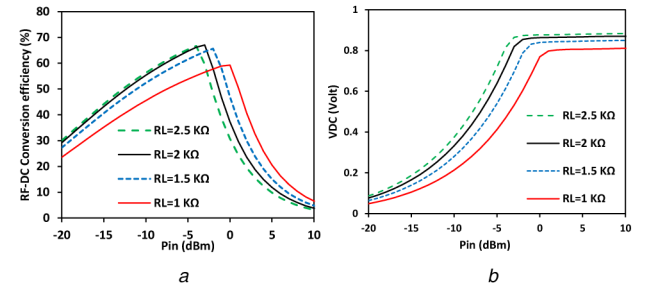


**Fig. 13 Study of changing  $R_L$  at  $f_2$**   
 (a) RF-DC conversion efficiency, (b) DC output voltage

between the antenna and rectifier circuit as shown in the fabricated prototype in Fig. 14. From the results that are presented in Fig. 15, it can be seen that a maximum measured conversion efficiency is improved to be about 74 and 70%, at  $f_1$  and  $f_2$ , with low input power levels of  $-6.5$  and  $-4.5$  dBm, respectively. The corresponding DC output voltages with sweeping of the incident input power are shown in Fig. 15 using the harmonic balance simulation. Also, the rectenna offers a wide band of input power with high sensitivity reach up to 47 and 36% at  $f_1$  and  $f_2$ , respectively, with an input power level of  $-20$  dBm. The measured values of the RF-DC conversion efficiency as a function of the input received power are greater than 50% from  $-18$  to  $-3.5$  dBm and from  $-15$  to  $-1.5$  dBm at the two operating frequencies as illustrated in Fig. 15.

The experimental setup that is used in the measurements is illustrated in Fig. 14. In order to generate the RF incident power on the rectenna, an Agilent E8257D signal generator in addition to horn antenna as a transmitting antenna with an average gain of 8 dB at the operating rectenna frequencies have been used. Measurements were carried out by placing the proposed rectenna at a distance of 50 cm from the transmitting horn antenna to guarantee the operating in the far-field region.

Friis transmission equation is used through the rectenna measurements to include the antenna radiation characteristics into the calculations. The rectenna conversion efficiency is calculated using (1), and the received power ( $P_{in}$ ) can be measured using (2). Also, the received power density ( $P_D$ ) is calculated from (3) and it in turn depends on the antenna effective area ( $A_{eff}$ ) defined in (4).

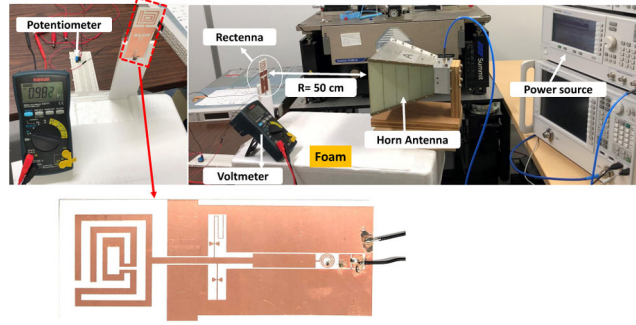


Fig. 14 Rectenna measurements setup

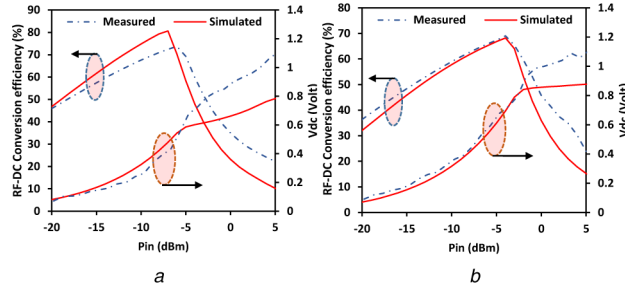


Fig. 15 Rectenna measured and simulated results of RF-DC conversion efficiency and DC output voltage at (a)  $f_1$ , (b)  $f_2$

Table 1 Comparison with some published papers

Ref.	Rectifier topology	Frequency	Maximum efficiency	Input power level at max. eff.	Sensitivity (at efficiency)	DC output voltage at max. eff., V	$R_L$	Diode
[5]	series connection	triple-band 900, 1800 and 2100 MHz	N/A	N/A	500 $\mu\text{W}/\text{m}^2$ (40%)	0.6	5 k $\Omega$	Skyworks SMS7630-079
[6]	single-stage Cockcroft Walton	single band 2.45 GHz	68%	5 dBm	-20 dBm(19%)	3.89	5 k $\Omega$	Avago HSMS2850
[8]	series connection	dual-band 915 MHz and 2.45 GHz	48 and 39%	0 dBm	-9dBm(37%, 30%)	—	2.2 k $\Omega$	Skyworks SMS7630
[10]	series connection	dual-band 850 and 1850 MHz	35 and 44%	-2 dBm	-20 dBm(15%)	0.03	2.2 k $\Omega$	Skyworks SMS7630
[12]	single-series	dual-band 0.9 and 1.8 GHz	38.1 and 34%	-20 dBm	-30 dBm (14.6 and 12.3%)	—	7 k $\Omega$	Avago HSMS-2850
[13]	single series	triple-band 1.84, 2.14 and 2.45 GHz	43.4, 46.5 and 38.4%	-10 dBm	-30 dBm(7.6, 8.6 and 4.3%)	0.13	5 k $\Omega$	Avago HSMS-2850
[16]	voltage doubler	single band 2.45 GHz	52%	0 dBm	-10 dBm (24%)	—	4 k $\Omega$	Avago HSMS2852
[20]	two-stage Cockcroft Walton	single band 900 MHz	58.7%	-10 dBm	-10dBm(58.7%)	—	10 M $\Omega$	Avago HSMS286Y
[21]	voltage doubler	triple band 2, 2.5 and 3.5 GHz	53, 31 and 15.56%	-13 and -12 dBm	-13 dBm(53%)	—	1.1 k $\Omega$	Avago HSMS285C
[22]	voltage doubler	dual band 1.95 and 2.5 GHz	63 and 69%	7 and 3.5 dBm	-3.5 dBm(50%), -4.5 dBm(50%)	2.5	1 k $\Omega$	Avago HSMS2850
this work	series connection	dual-band 700 and 1400 MHz	74 and 70%	-6.5 and -4.5 dBm	-20 dBm (47 and 36%)	0.7	1.9 k $\Omega$	Skyworks SMS7630-061

Therefore, the received input power can be calculated from (4) and in dB from (5). CL is the cable loss in dB,  $P_t$ ,  $G_t$  and  $G_r$  are in dB. Table 1 shows a comparison between the proposed rectenna and recently published rectennas. The proposed rectenna shows a high sensitivity and higher RF-DC conversion efficiency among the other research papers

$$P_{in} = P_D \times A_{eff} \quad (2)$$

$$P_D = \frac{P_t G_t}{4\pi r^2} \quad (3)$$

$$A_{eff} = G_r \frac{\lambda^2}{4\pi} \quad (4)$$

$$\therefore P_{in} = P_t G_t G_r \left(\frac{\lambda}{4\pi r}\right)^2 \quad (5)$$

$$P_{in}(\text{dB}) = P_t + G_t + G_r + 20\log_{10}\left(\frac{\lambda}{4\pi r}\right) + \text{CL} \quad (6)$$

## 5 Conclusion

A dual-band CPW rectenna for low input received power energy harvesting applications is proposed in this research work. The rectenna has high sensitivity reach up to  $-20$  dBm with a high measured RF-DC conversion efficiency of 47%. The antenna, as well as the rectifier circuit, are designed and tested separately. Finally, the matching circuit is designed and the integration is done on the same PCB substrate.

## 6 References

- [1] Wang, G., Liu, W., Sivaprakasam, M., *et al.*: 'Design and analysis of an adaptive transcutaneous power telemetry for biomedical implants', *IEEE Trans. Circuits Syst. I, Regul. Pap.*, 2005, **52**, (10), pp. 2109–2117
- [2] Nguyen, V.T., Kang, S.H., Choi, J.H., *et al.*: 'Magnetic resonance wireless power transfer using three-coil system with single planar receiver for laptop applications', *IEEE Trans. Consum. Electron.*, 2015, **61**, (2), pp. 160–166
- [3] Low, Z.N., Chinga, R.A., Tseng, R., *et al.*: 'Design and test of a high-power high-efficiency loosely coupled planar wireless power transfer system', *IEEE Trans. Ind. Electron.*, 2009, **56**, (5), pp. 1801–1812
- [4] 'Solutions P: Wireless charging pad, black sapphire. Samsung mobile accessories' Available at <http://www.powemat.com>
- [5] Shen, S., Chiu, C.Y., Murch, R.D.: 'A dual-port triple-band l-probe microstrip patch rectenna for ambient RF energy harvesting', *IEEE Antennas Wirel. Propag. Lett.*, 2017, **16**, pp. 3071–3074
- [6] Awais, Q., Jin, Y., Chattha, H.T., *et al.*: 'A compact rectenna system with high conversion efficiency for wireless energy harvesting', *IEEE Access*, 2018, **6**, pp. 35857–35866
- [7] Khemar, A., Kacha, A., Takhedmit, H., *et al.*: 'Design and experiments of a dual-band rectenna for ambient RF energy harvesting in urban environments', *IET Microw. Antennas Propag.*, 2017, **12**, (1), pp. 49–55
- [8] Niotaki, K., Kim, S., Jeong, S., *et al.*: 'A compact dual-band rectenna using slot-loaded dual band folded dipole antenna', *IEEE Antennas Wirel. Propag. Lett.*, 2013, **12**, pp. 1634–1637
- [9] Sun, H., Guo, Y.X., He, M., *et al.*: 'A dual-band rectenna using broadband yagi antenna array for ambient RF power harvesting', *IEEE Antennas Wirel. Propag. Lett.*, 2013, **12**, pp. 918–921
- [10] Collado, A., Georgiadis, A.: 'Conformal hybrid solar and electromagnetic (em) energy harvesting rectenna', *IEEE Trans. Circuits Syst.*, 2013, **60**, (8), pp. 2225–2234
- [11] Noghabaei, S.M., Radin, R.L., Savaria, Y., *et al.*: 'A high-efficiency ultra-low-power cmos rectifier for RF energy harvesting applications'. 2018 IEEE Int. Symp. on Circuits and Systems (ISCAS), IEEE, Florence, Italy, 2018, pp. 1–4
- [12] Shen, S., Zhang, Y., Chiu, C., *et al.*: 'An ambient rf energy harvesting system where the number of antenna ports is dependent on frequency', *IEEE Trans. Microw. Theory Tech.*, 2019, **67**, (9), pp. 3821–3832
- [13] Shen, S., Zhang, Y., Chiu, C., *et al.*: 'A triple-band high-gain multibeam ambient rf energy harvesting system utilizing hybrid combining', *IEEE Trans. Ind. Electron.*, 2019, pp. 1–1
- [14] Scheeler, R., Korhummel, S., Popovic, Z.: 'A dual-frequency ultralow-power efficient 0.5-g rectenna', *IEEE Microw. Mag.*, 2014, **15**, (1), pp. 109–114
- [15] Song, C., Huang, Y., Zhou, J., *et al.*: 'Matching network elimination in broadband rectennas for high-efficiency wireless power transfer and energy harvesting', *IEEE Trans. Ind. Electron.*, 2017, **64**, (5), pp. 3950–3961
- [16] Shi, Y., Jing, J., Fan, Y., *et al.*: 'Design of a novel compact and efficient rectenna for wifi energy harvesting', *Prog. Electromagn. Res.*, 2018, **83**, pp. 57–70
- [17] Song, C., Huang, Y., Zhou, J., *et al.*: 'A high-efficiency broadband rectenna for ambient wireless energy harvesting', *IEEE Trans. Antennas Propag.*, 2015, **63**, (8), pp. 3486–3495
- [18] Ladan, S., Guntupalli, A.B., Wu, K.: 'A high-efficiency 24 ghz rectenna development towards millimeter-wave energy harvesting and wireless power transmission', *IEEE Trans. Circuits Syst. I, Regul. Pap.*, 2014, **61**, (12), pp. 3358–3366
- [19] Marian, V., Vollaie, C., Allard, B., *et al.*: 'Low power rectenna topologies for medium range wireless energy transfer'. Proc. of the 2011 14th European Conf. on Power Electronics and Applications, Birmingham, UK., 2011, pp. 1–10
- [20] Kanaya, H., Tsukamaoto, S., Hirabaru, T., *et al.*: 'Energy harvesting circuit on a one-sided directional flexible antenna', *IEEE Microw. Wirel. Compon. Lett.*, 2013, **23**, (3), pp. 164–166
- [21] Chandravanshi, S., Sarma, S.S., Akhtar, M.J.: 'Design of triple band differential rectenna for rf energy harvesting', *IEEE Trans. Antennas Propag.*, 2018, **66**, (6), pp. 2716–2726
- [22] Aboualalaa, M., Mansour, I., Abdel Rahman, A.B., *et al.*: 'Dual-band rectenna using voltage doubler rectifier and four-section matching network'. IEEE MTT-S Wireless Power Transfer, Montreal, Canada, 2018